JACS
JOURNAL OF THE AMERICAN CHEMICAL SOCIETY
Communication
pubs.acs.org/JACS

Superconductivity in $KCa_2Fe_4As_4F_2$ with Separate Double Fe_2As_2 Layers

Zhi-Cheng Wang,[†] Chao-Yang He,[†] Si-Qi Wu,[†] Zhang-Tu Tang,[†] Yi Liu,[†] Abduweli Ablimit,[†] Chun-Mu Feng,[†] and Guang-Han Cao*[,†,‡]

[†]Department of Physics and State Key Lab of Silicon Materials, Zhejiang University, Hangzhou 310027, China
[‡]Collaborative Innovation Centre of Advanced Microstructures, Nanjing 210093, China

Supporting Information

ABSTRACT: We report the synthesis, crystal structure, and physical properties of a quinary iron arsenide fluoride, $KCa_2Fe_4As_4F_2$. The new compound crystallizes in a body-centered tetragonal lattice (space group $I4/mmm$, a = 3.8684(2) Å, c = 31.007(1) Å, Z = 2) that contains double Fe_2As_2 conducting layers separated by insulating Ca_2F_2 layers. Our measurements of electrical resistivity, direct-current magnetic susceptibility, and heat capacity demonstrate bulk superconductivity at 33 K in $KCa_2Fe_4As_4F_2$.

Currently, only cuprate and iron-based superconductors exhibit ambient-pressure high-temperature superconductivity.[1,2] The two classes of materials share many similarities.[3] Structurally, for example, they are quasi-two-dimensional, possessing superconductively active CuO_2 planes and Fe_2As_2 layers, respectively. This feature makes it possible to "design" a new superconductor by replacing the crystallographic spacer layers.[4,5] However, all of the Fe-based superconductors (FeSCs) discovered to date consist of separate Fe_2As_2 monolayers or infinite Fe_2As_2 layers [such as the case of $(Ba,K)Fe_2As_2$]. By contrast, many cuprate superconductors contain separate multi-CuO_2 planes, which may optimize the superconducting transition temperature T_c.[3,4]

On the basis of an understanding of the crystal chemistry of FeSCs, especially in terms of the "hard and soft acids and bases" (HSAB)[6] concept, we proposed a rational structural design in search of new FeSCs.[5] Nine structures containing Fe_2X_2 (X = pnictogen or chalcogen) layers were suggested to be the candidates. Among them, the one with a chemical formula of $A_3Fe_4X_4Z_2$,[5] where A represents a "hard" cation (there are two distinct crystallographic sites for A) and Z denotes a "hard" anion, contains separate double Fe_2As_2 layers. According to the HSAB rule,[6] AZ and FeX are expected to combine together to form fluorite-like and antifluorite-like layers, respectively. Figure 1 shows an example of $A_3Fe_4X_4Z_2$, namely, the title compound $KCa_2Fe_4As_4F_2$. The crystal structure is actually an intergrowth of ZrCuSiAs-type CaFeAsF and $ThCr_2Si_2$-type KFe_2As_2. Indeed, the crystallographic building unit $[KFe_4As_4]^{2-}$ (highlighted by the red rectangular block in the middle of Figure 1) contains double Fe_2As_2 layers (with K atoms sandwiched) separated by Ca_2F_2 layers, precisely resembling the double CuO_2 planes in cuprates exemplified by $La_{2-x}Sr_xCaCu_2O_6$.[7] The analogous crystal structure was reported earlier in Cu- and Ni-based pnictides,[8] but to the best of our knowledge, their Fe-based counterpart has not been synthesized until now. In this Communication, we report the synthesis, crystal structure, and superconductivity of $KCa_2Fe_4As_4F_2$. As a result of the intergrowth structure, the Fe_2As_2 layers with different cations aside are no longer symmetric. The material is hole-doped by itself, which yields a superconducting transition temperature (T_c) of 33 K.

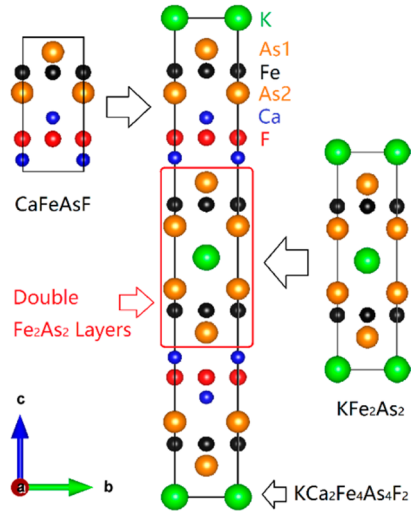

Figure 1. Crystal structure of $KCa_2Fe_4As_4F_2$ with separate double Fe_2As_2 layers (highlighted with the red rectangular block in the middle) resulting from intergrowth of CaFeAsF (left) and KFe_2As_2 (right).

The $KCa_2Fe_4As_4F_2$ polycrystalline sample was synthesized via solid-state reactions of presynthesized/pretreated KAs, CaF_2, CaAs, and Fe_2As in an evacuated container. First, the intermediate binary products KAs, CaAs, and Fe_2As were prepared by solid-state reactions of their corresponding elements at 250, 750, and 750 °C, respectively, in evacuated quartz tubes. The source materials were K cubes (99.5%), redistilled Ca granules (99.5%), Fe powder (99.998%), As pieces (99.999%), and CaF_2 powder (99.5%). CaF_2 was heated to 500 °C for 12 h in a muffle furnace to remove adsorbed water. Second, stoichiometric mixtures of KAs, CaF_2, CaAs, and Fe_2As were pressed into pellets, and the pellets were loaded in an alumina tube with a cover. Then the sample-loaded alumina

Received: May 2, 2016
Published: June 20, 2016

DOI: 10.1021/jacs.6b04538
J. Am. Chem. Soc. 2016, 138, 7856−7859

tube was sealed in a Ta tube, which was jacketed with an evacuated quartz ampule. The sample assembly was sintered at 930 °C for 36 h. Third, the solid-state reaction was repeated, with a sample homogenization by grinding, in order to improve the quality of the sample. The final product is stable in air.

We employed energy-dispersive X-ray (EDX) spectroscopy to verify the chemical composition of the title compound. The results show that the crystalline grains are indeed composed of K, Ca, Fe, As, and F, whose atomic ratios basically meet the expected chemical formula (see Figure S1 and Table S1 in the Supporting Information). Powder X-ray diffraction (XRD) experiments were conducted at room temperature on a PANalytical X-ray diffractometer with Cu Kα1 radiation. On the basis of the structural model shown in Figure 1, the crystal structure was refined by a Rietveld analysis using RIETAN software.[9] The resulting weighted reliability factor (R_{wp}) was 4.04% and the goodness of fit χ^2 was 1.85, indicating reliability of the refinement.

The electrical resistivity (ρ), Hall coefficient (R_H), and heat capacity (C) measurements were carried out on a Quantum Design Physical Property Measurement System (PPMS-9). We employed the ac transport option for the $\rho(T, H)$ and $R_H(T)$ measurements. The $C(T, H)$ data were measured by a thermal relaxation method using a square-shaped sample plate (13.1 mg). The direct-current (dc) magnetization was measured on a Quantum Design Magnetic Property Measurement System (MPMS-XL5). The sample was polished into a rod whose demagnetization factor is 0.14. Both zero-field cooling (ZFC) and field-cooling (FC) protocols were adopted to probe the superconducting transition.

The XRD pattern of the as-prepared sample can be indexed well with a body-centered tetragonal lattice. Impurity phases of KFe_2As_2, FeAs, and CaF_2 can be identified, but their strongest lines are only 3.0%, 2.0%, and 1.8%, respectively, of the strongest reflection of the main phase. We then carried out a three-phase Rietveld refinement (the reflection lines of CaF_2 were taken as an internal standard, which was not included for the refinement), as shown in Figure 2. The results show that the mass percentage of the main phase $KCa_2Fe_4As_4F_2$ is 93.4%. Table 1 lists the refined crystallographic data for $KCa_2Fe_4As_4F_2$. The a lattice constant lies between those of KFe_2As_2 (3.842 Å)[10] and CaFeAsF (3.878 Å).[11] Meanwhile, the

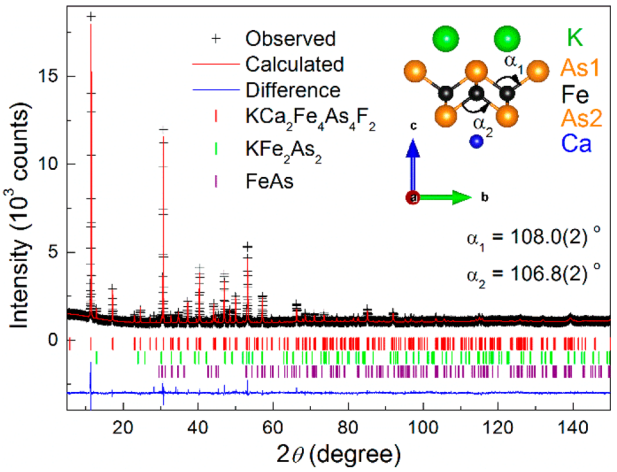

Figure 2. Multiple-phase Rietveld refinement profile of powder XRD data for the $KCa_2Fe_4As_4F_2$ sample. The inset shows the refined structure of the Fe_2As_2 layer projected along the [100] direction.

Table 1. Crystallographic Data for $KCa_2Fe_4As_4F_2$ (Space Group $I4/mmm$, No. 139) at Room Temperature; The Lattice Parameters are a = 3.8684(2) Å and c = 31.007(1) Å

atom	site	x	y	z	Occ.[a]	B_{iso}[b]
K	2a	0	0	0	1.0	1.2 (3)
Ca	4e	0	0	0.2085(2)	1.0	0.2
Fe	8g	0	0.5	0.1108(1)	1.0	0.2
As1	4e	0	0	0.0655(1)	1.0	0.4 (1)
As2	4e	0	0	0.1571(1)	1.0	0.3 (1)
F	4d	0	0.5	0.25	1.0	1.0

[a]The occupancy of each atom was fixed to be 1.0 in the Rietveld refinement. [b]The temperature factors of Ca, Fe, and F were fixed to avoid an unphysical negative value.

c lattice constant is noticeably smaller than, yet very close to, the sum (31.05 Å) of that of KFe_2As_2 (13.861 Å)[10] and twice of that of CaFeAsF (2 × 8.593 Å),[11] consistent with the proposed intergrowth "12442" structure in Figure 1. The shrinkage of c suggests stabilization of the intergrowth phase. While the thickness of the "KFe_2As_2" block is obviously shortened (from 6.931 to 6.871 Å), the length of the "CaFeAsF" unit is elongated appreciably (from 8.593 to 8.632 Å). This structural variation is associated with charge redistribution, because the Fe valence turns into 2.25+ instead of being either 2+ as in CaFeAsF or 2.5+ as in KFe_2As_2. Similar charge homogenization appears in $AeAFe_4As_4$ (Ae = Ca, Sr; A = K, Rb, Cs)[12] and $RbEuFe_4As_4$[13] (1144-type) superconductors discovered very recently.

It is the hybridized structure that makes the Fe_2As_2 layers asymmetric, unlike most FeSCs, which possess Fe_2As_2 layers with S_4 symmetry. Such an asymmetric Fe coordination was first observed in the 1144-type superconductors[12,13] (but these FeSCs still contain infinite Fe_2As_2 layers). In FeSCs, the height of As from the Fe plane and the As−Fe−As bond angle (α) are considered to be the two relevant structural parameters that determine T_c.[14,15] Here, the As1 (nearby K) and As2 (nearby Ca) heights are 1.405(3) and 1.436 (3) Å, respectively, which seem to meet a T_c value of about 30 K. Meanwhile, the As1−Fe−As1 and As2−Fe−As2 bond angles are 108.0(2)° and 106.8(2)°, respectively, both of which are not far from the ideal value of 109.5° for acquiring an optimized T_c.

Figure 3 shows the resistivity measurement results for the polycrystalline $KCa_2Fe_4As_4F_2$ sample. The $\rho(T)$ curve exhibits metallic behavior above T_c. A broad hump appears at around 175 K, which is very often seen in hole-doped FeSCs.[16−18] This phenomenon can be explained in terms of an incoherent-to-coherent crossover, which has very recently been revealed as an emergent Kondo lattice behavior in heavily hole-doped $AkFe_2As_2$ (Ak = K, Rb, Cs).[18] The hole-doping scenario is unambiguously demonstrated by the Hall measurements which show positive $R_H(T)$ values above T_c (see Figure S2). Below 100 K, the resistivity decreases almost linearly until superconductivity emerges. The superconducting transition is clearly shown in Figure 3b, where the onset, midpoint, and zero-resistance temperatures were determined to be 33.1, 32.8, and 32.3 K, respectively. It should be noted that the temperature at which $\rho(T)$ deviates from linearity is as high as 35 K, indicating a strong superconducting thermal fluctuation. Similar phenomenon is observed in $Sr_2VFeAsO_3$ which hosts a very weak interlayer coupling because of the thick spacer layers.[19] Here the weak interlayer coupling seems to be related to the body-

DOI: 10.1021/jacs.6b04538
J. Am. Chem. Soc. 2016, 138, 7856−7859

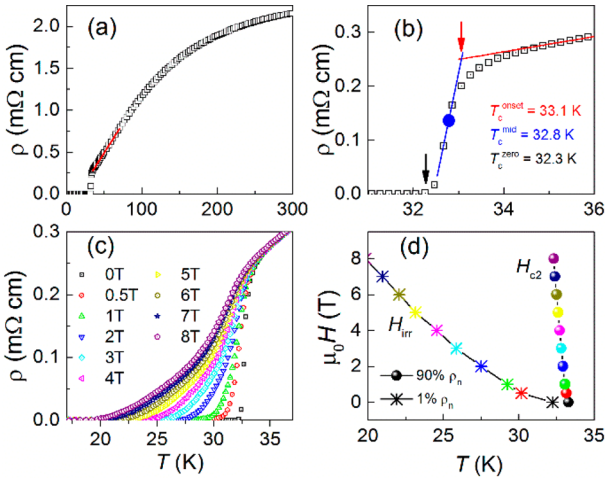

Figure 3. (a–c) Temperature dependence of the resistivity for the $KCa_2Fe_4As_4F_2$ polycrystalline sample. (d) Derived upper critical field (H_{c2}) and irreversible field (H_{irr}).

centered lattice because the adjacent Fe_2As_2 double layers mutually shift by ($^1/_2$, $^1/_2$, 0).

Upon the application of magnetic fields, the superconducting transitions shift to lower temperatures, as shown in Figure 3c. Impressively, the superconducting transition severely broadens with a pronounced tail under a magnetic field, similar to the case of $Sr_2VFeAsO_3$.[19] Using a conventional criteria of 90% of ρ_n (where ρ_n refers to the linearly extrapolated normal-state resistivity at T_c under zero field) for determining the upper critical field (H_{c2}) and 1% of ρ_n for the irreversible field (H_{irr}), we obtained a superconducting phase diagram (Figure 3d). The slope of $H_{c2}(T)$ is as high as 8.4 T K^{-1}, suggesting a small superconducting coherence length at zero temperature. The large gap between $H_{c2}(T)$ and $H_{irr}(T)$ implies a high anisotropy owing to the weak interlayer coupling. Future measurements under very high magnetic fields and using single-crystal samples may give an accurate and expanded superconducting phase diagram.

Superconductivity in $KCa_2Fe_4As_4F_2$ was confirmed by the dc magnetic susceptibility (χ) measurements. As shown in Figure 4, the onset diamagnetic transition temperature is 33 K, consistent with the resistivity measurement above. The upper

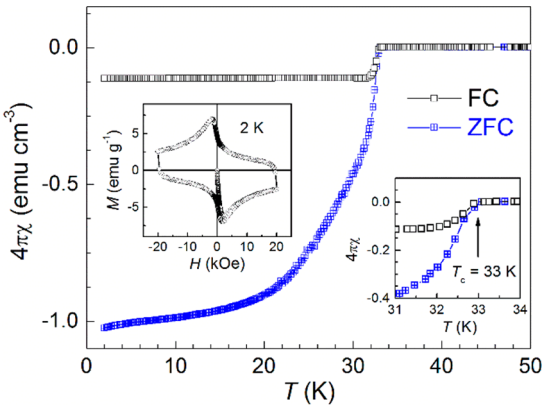

Figure 4. Temperature dependence of the magnetic susceptibility measured at 10 Oe for $KCa_2Fe_4As_4F_2$. The left inset shows the isothermal magnetization loop at 2 K, and the right inset zooms in on the superconducting transition.

limit of the superconducting volume fraction, measured in the ZFC process, reaches 100% at temperatures far below T_c after a demagnetization correction is made. On the other hand, the volume fraction of magnetic repulsion, measured in the FC process, is remarkably reduced because of a magnetic flux pinning effect, which is clearly demonstrated by the isothermal magnetization at 2 K (shown in the left inset in Figure 4). Even so, the magnetic repulsion fraction (11%), a lower limit of the superconducting volume fraction, is still higher than any impurity content in the sample (in fact, none of the identified impurities are possibly superconducting at 33 K). Therefore, $KCa_2Fe_4As_4F_2$ is unambiguously responsible for the 33 K superconductivity. It should be noted that there is a detectable kink at about 4 K, close to the superconducting transition of KFe_2As_2.[17] The magnitude of the decrease in $4\pi\chi$ (down to 2.0 K) is about 2%, satisfying the KFe_2As_2 content from the XRD results above.

Figure 5 shows the specific heat capacity for $KCa_2Fe_4As_4F_2$. An obvious specific-heat jump at T_c = 33 K can be seen in the

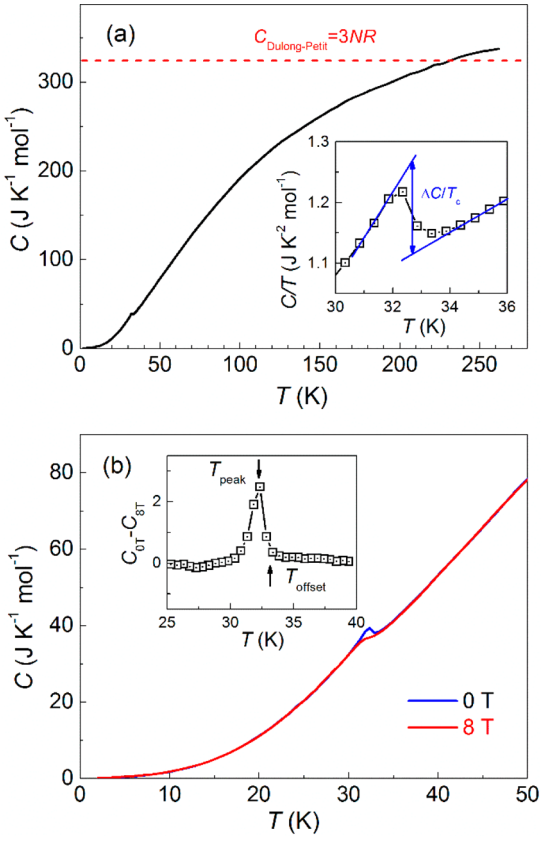

Figure 5. (a) Specific heat $C(T)$ over the whole temperature range for $KCa_2Fe_4As_4F_2$. The inset presents a plot of C/T vs T over a narrow temperature range, showing a specific-heat jump at T_c. (b) Comparison of the $C(T)$ data under magnetic fields of μ_0H = 0 and 8 T. Their difference is displayed in the inset.

inset of Figure 5a, further confirming the bulk superconductivity. The thermodynamic transition temperature is 32.7 K based on an entropy-conserving construction. Under a magnetic field of 8 T, the specific-heat jump is remarkably suppressed (Figure 5b). As a result, the difference in $C(T)$ exhibits a peak at around T_c. The thermodynamic transition temperature is lowered by 0.5 K at 8 T. If the thermodynamic transitions for determining H_{c2} are used, the initial slope of

DOI: 10.1021/jacs.6b04538
J. Am. Chem. Soc. 2016, 138, 7856–7859

$H_{c2}(T)$ can be as high as 16 T K^{-1}. As mentioned above, measurements on the single crystals will be able to clarify this discrepancy.

The magnitude of the specific-heat jump scaled by T_c achieves $\Delta C/T_c$ = 150 mJ K^{-2} mol^{-1} (or 38 mJ K^{-2} (mol of Fe)$^{-1}$). In the Bardeen−Cooper−Schrieffer weak-coupling scenario, the dimensionless parameter $\Delta C/(\gamma T_c)$ is equal to 1.43, where γ denotes the normal-state electronic specific-heat coefficient. If so, the γ value can be estimated to be 105 mJ K^{-2} mol^{-1} (equivalent to 26 mJ K^{-2} (mol of Fe)$^{-1}$). This large γ value explains the high-temperature $C(T)$ data that unusually exceed the Dulong−Petit limit. It is noted here that the enhanced γ is not unusual for hole-doped FeSCs.[13,20]

As is known, most FeSCs are realized through chemical doping in so-called parent compounds.[3,5] Here the occurrence of superconductivity in $KCa_2Fe_4As_4F_2$ is also due to hole doping, yet by the material itself, as the constituents of $KCa_2Fe_4As_4F_2$, namely, CaFeAsF[11] and KFe_2As_2,[17] are a parent compound and a 3.8 K superconductor, respectively. The structural hybridization changes the Fe valence to 2.25+, as mentioned above. This means that the title compound is actually hole-doped to a level of 0.25 hole/Fe. Indeed, the Hall carrier number is estimated to be 0.18 hole/Fe assuming a single-band scenario and employing the Hall coefficient value at 100 K (Figure S2). It should be noted that a similar self-doping effect, albeit via an internal charge transfer, has been found in other systems, including $Sr_2VFeAsO_3$,[21] $Ba_2Ti_2Fe_2As_4O$,[22] and $Eu_3Bi_2S_4F_4$.[23] One may expect that such a self-doping strategy could be continually utilized for future exploration of superconductors.

Finally, we remark on the prospect of our finding. In the 12442-type superconductor, there are five different crystallographic sites, which are suitably occupied by different types of elements according to the HSAB classification. Hence, there are a lot of combinations for element replacements in $KCa_2Fe_4As_4F_2$. Hopefully, more 12442-type superconductors will be found through simple element replacements in the near future.

■ ASSOCIATED CONTENT

Supporting Information

The Supporting Information is available free of charge on the ACS Publications website at DOI: 10.1021/jacs.6b04538.

Typical EDX spectrum of $KCa_2Fe_4As_4F_2$, Hall measurement results, and quantitative analysis of the EDX spectra (PDF)

Crystallographic data for $KCa_2Fe_4As_4F_2$ (CIF)

■ AUTHOR INFORMATION

Corresponding Author

*ghcao@zju.edu.cn

Notes

The authors declare no competing financial interest.

■ ACKNOWLEDGMENTS

This work was supported by the National Natural Science Foundation of China (Grants 11190023 and 90922002) and the Fundamental Research Funds for the Central Universities of China.

■ REFERENCES

(1) (a) Bednorz, J. G.; Muller, K. A. *Z. Phys. B: Condens. Matter* **1986**, *64*, 189. (b) Wu, M. K.; Ashburn, J. R.; Torng, C. J.; Hor, P. H.; Meng, R. L.; Gao, L.; Huang, Z. J.; Wang, Y. Q.; Chu, C. W. *Phys. Rev. Lett.* **1987**, *58*, 908.

(2) (a) Kamihara, Y.; Watanabe, T.; Hirano, M.; Hosono, H. *J. Am. Chem. Soc.* **2008**, *130*, 3296. (b) Chen, X. H.; Wu, T.; Wu, G.; Liu, R. H.; Chen, H.; Fang, D. F. *Nature* **2008**, *453*, 761.

(3) Scalapino, D. J. *Rev. Mod. Phys.* **2012**, *84*, 1383.

(4) Raveau, B.; Michel, C.; Hervieu, M.; Groult, D. In *Crystal Chemistry of High T_c Superconducting Copper Oxides*; Springer: Berlin, 1991.

(5) Jiang, H.; Sun, Y. L.; Xu, Z. A.; Cao, G. H. *Chin. Phys. B* **2013**, *22*, 087410.

(6) Pearson, R. G. *J. Am. Chem. Soc.* **1963**, *85*, 3533.

(7) Cava, R. J.; Batlogg, B.; van Dover, R. B.; Krajewski, J. J.; Waszczak, J. V.; Fleming, R. M.; Peck, W. F., Jr; Rupp, L. W., Jr; Marsh, P.; James, A. C. W.; Schneemeyer, L. F. *Nature* **1990**, *345*, 602.

(8) (a) Cava, R. J.; Zandbergen, H. W.; Krajewski, J. J.; Siegrist, T.; Hwang, H. Y.; Batlogg, B. *J. Solid State Chem.* **1997**, *129*, 250. (b) Klimczuk, T.; McQueen, T. M.; Williams, A. J.; Huang, Q.; Ronning, F.; Bauer, E. D.; Thompson, J. D.; Green, M. A.; Cava, R. J. *Phys. Rev. B: Condens. Matter Mater. Phys.* **2009**, *79*, 012505. (c) Wang, J. K.; Marcinkova, A.; Chen, C. W.; He, H.; Aronson, M.; Morosan, E. *Phys. Rev. B: Condens. Matter Mater. Phys.* **2014**, *89*, 094405.

(9) Izumi, F.; Momma, K. *Solid State Phenom.* **2007**, *130*, 15.

(10) Rozsa, S.; Schuster, H.-U. *Z. Naturforsch., B: J. Chem. Sci.* **1981**, *36*, 1668.

(11) Matsuishi, S.; Inoue, Y.; Nomura, T.; Yanagi, H.; Hirano, M.; Hosono, H. *J. Am. Chem. Soc.* **2008**, *130*, 14428.

(12) Iyo, A.; Kawashima, K.; Kinjo, T.; Nishio, T.; Ishida, S.; Fujihisa, H.; Gotoh, Y.; Kihou, K.; Eisaki, H.; Yoshida, Y. *J. Am. Chem. Soc.* **2016**, *138*, 3410.

(13) Liu, Y.; Liu, Y. B.; Tang, Z. T.; Jiang, H.; Wang, Z. C.; Ablimit, A.; Jiao, W. H.; Tao, Q.; Feng, C. M.; Xu, Z. A.; Cao, G. H. *Phys. Rev. B: Condens. Matter Mater. Phys.* **2016**, *93*, 214503.

(14) Mizuguchi, Y.; Hara, Y.; Deguchi, K.; Tsuda, S.; Yamaguchi, T.; Takeda, K.; Kotegawa, H.; Tou, H.; Takano, Y. *Supercond. Sci. Technol.* **2010**, *23*, 054013.

(15) (a) Lee, C. H.; Iyo, A.; Eisaki, H.; Kito, H.; Fernandez-Diaz, M. T.; Ito, T.; Kihou, K.; Matsuhata, H.; Braden, M.; Yamada, K. *J. Phys. Soc. Jpn.* **2008**, *77*, 083704. (b) Zhao, J.; Huang, Q.; de la Cruz, C.; Li, S.; Lynn, J. W.; Chen, Y.; Green, M. A.; Chen, G. F.; Li, G.; Li, Z.; Luo, J. L.; Wang, N. L.; Dai, P. *Nat. Mater.* **2008**, *7*, 953.

(16) Rotter, M.; Tegel, M.; Johrendt, D. *Phys. Rev. Lett.* **2008**, *101*, 107006.

(17) Sasmal, K.; Lv, B.; Lorenz, B.; Guloy, A. M.; Chen, F.; Xue, Y. Y.; Chu, C. W. *Phys. Rev. Lett.* **2008**, *101*, 107007.

(18) Wu, Y. P.; Zhao, D.; Wang, A. F.; Wang, N. Z.; Xiang, Z. J.; Luo, X. G.; Wu, T.; Chen, X. H. *Phys. Rev. Lett.* **2016**, *116*, 147001.

(19) Zhu, X.; Han, F.; Mu, G.; Cheng, P.; Shen, B.; Zeng, B.; Wen, H. H. *Phys. Rev. B: Condens. Matter Mater. Phys.* **2009**, *79*, No. 220512(R).

(20) Mu, G.; Luo, H.; Wang, Z.; Shan, L.; Ren, C.; Wen, H. H. *Phys. Rev. B: Condens. Matter Mater. Phys.* **2009**, *79*, 174501.

(21) Cao, G. H.; Ma, Z. F.; Wang, C.; Sun, Y. L.; Bao, J. K.; Jiang, S.; Luo, Y. K.; Feng, C. M.; Zhou, Y.; Xie, Z.; Hu, F. C.; Wei, S. Q.; Nowik, I.; Felner, I.; Zhang, L.; Xu, Z. A.; Zhang, F. C. *Phys. Rev. B: Condens. Matter Mater. Phys.* **2010**, *82*, 104518.

(22) Sun, Y. L.; Jiang, H.; Zhai, H. F.; Bao, J. K.; Jiao, W. H.; Tao, Q.; Shen, C. Y.; Zeng, Y. W.; Xu, Z. A.; Cao, G. H. *J. Am. Chem. Soc.* **2012**, *134*, 12893.

(23) Zhai, H. F.; Zhang, P.; Wu, S. Q.; He, C. Y.; Tang, Z. T.; Jiang, H.; Sun, Y. L.; Bao, J. K.; Nowik, I.; Felner, I.; Zeng, Y. W.; Li, Y. K.; Xu, X. F.; Tao, Q.; Xu, Z. A.; Cao, G. H. *J. Am. Chem. Soc.* **2014**, *136*, 15386.

DOI: 10.1021/jacs.6b04538
J. Am. Chem. Soc. 2016, 138, 7856−7859